Spectrochimica Acta Part A: Molecular and Biomolecular Spectroscopy 311 (2024) 123997

Contents lists available at ScienceDirect

Spectrochimica Acta Part A:
Molecular and Biomolecular Spectroscopy

journal homepage: www.journals.elsevier.com/spectrochimica-acta-part-a-molecular-and-biomolecular-spectroscopy

Conformational isomerism in trans-3-methoxycinnamic acid: From solid to gas phase

Roger Castillo, Susana Blanco, Juan Carlos López *

Departamento de Química Física y Química Inorgánica, IU CINQUIMA, Facultad de Ciencias, Universidad de Valladolid, Valladolid, Spain

HIGHLIGHTS

- Laser ablation seeding into a supersonic jet bring the single stable conformation of solid trans-3-methoxycynnamic acid into a mixture of eight cooled conformers.
- The full conformational panorama of trans-3-methoxycynnamic acid in the gas phase was investigated by microwave spectroscopy.
- The rich conformational dynamics of trans-3-methoxycynnamic acid is due to the rotatable single bonds.

GRAPHICAL ABSTRACT

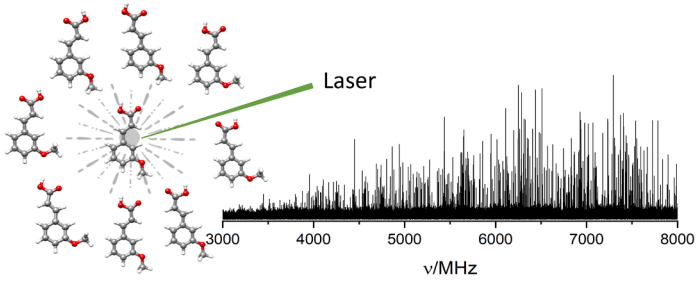

ARTICLE INFO

Keywords:
Trans-3-methoxycinnamic acid
Laser ablation
Rotational spectroscopy
Conformational isomerism

ABSTRACT

The rotational spectrum of laser ablated trans-3-methoxycinnamic acid has been observed in the 2–8 GHz range using chirped-pulse Fourier transform microwave spectroscopy coupled to a supersonic jet and adapted to support a laser ablation vaporization system (LA-CP-FTMW). Eight stable conformers were theoretically predicted to exist at B3LYP-D3BJ/6–311++(2d,p) level, all of which were experimentally detected. The experimental rotational parameters data evidence the essentially planar structures for all the conformers. The relative population distribution of conformers in the supersonic jet was investigated from relative intensity measurements. Cooling in the jet brings rotational temperatures close to 1 K for all the conformers. The theoretical predictions for the rotational constants and electric dipole moments show good agreement with the experimental constants and selection rules observed. The population distribution of conformers in the supersonic jet was found to be close to the equilibrium distribution calculated at temperatures lower than the stagnation temperature. Finally, the correlation of the observed conformers structures with those found in condensed phases was investigated.

1. Introduction

The number of conformations accessible to small biomolecules is of great interest in biochemistry and drug discovery, since the shape of a molecule is a major determinant of its biological and physical properties. The number of theoretically possible conformations of organic molecules is generally related to the torsion angles of their rotatable single bonds and the possible ring geometries. While many of these conformations are energetically unfavoured and are not observed experimentally there are molecules with a relatively large number of observable

* Corresponding author.
E-mail address: juancarlos.lopeza@uva.es (J.C. López).

https://doi.org/10.1016/j.saa.2024.123997
Received 25 October 2023; Received in revised form 30 January 2024; Accepted 3 February 2024
Available online 6 February 2024

conformers [1–5] for which conformational free energy differences can be related to their observed populations. Experimentally there are a wide range of techniques that cover structure determination in different conditions. Condensed phase structures have been investigated using NMR and X-ray crystallography. Crystal structures are deposited in the Cambridge Structural Database (CSD) [6]. In the context of drug research, the conformations of molecules bound to target macromolecules are important. The known structures of ligands bound to protein or pharmaceutical targets are collected in the Protein Data Bank (PDB) [7]. However, to reveal the complete conformational space associated to a molecule gas phase studies are needed. For example, a conformation observed in a crystal may be due to an unusually favourable intermolecular interaction which is not present in solution or in gas phase. While the complete conformational panorama of an isolated molecule can be only investigated theoretically using computational chemistry methods, the most populated conformations can be experimentally accessed in the gas phase using rotational spectroscopy techniques [1–5]. The correlation of the gas phase conformations with crystal or protein bound bioactive conformations would give a complete understanding of the properties of a molecule, since in many cases the conformation adopted by a molecule in condensed phase is accessible at a low energetical costs from the isolated molecule conformations [8,9].

The 3-(3-methoxyphenyl)-prop-2(E)-enoic acid, commonly known as trans-3-methoxycinnamic acid (3mca, Fig. 1), is a member of the wide family of cinnamic acid derivatives with pharmacological interest which potentially may adopt a wide range of molecular conformers/rotamers through the rotation about single bonds (Fig. 1). It has antioxidant properties [10] and has applications in leukemia [11], cancer [12], and diabetes [13] treatments. It also has antibacterial capacities [14] of application in the food industry, where it has been found useful as inhibitor of the enzymatic browning reactions in fruits damaged during manufacturing and post-harvest processing [15,16]. In the fields of inorganic and crystal chemistry, 3mca has been used, together with trans-2-methoxycinnamic acid (2mca), as a chelating agent in the synthesis of binuclear complex crystals and one-dimensional coordination polymers of rare earth elements with magnetic and luminescent properties [17,18]. Finally, it has been shown that 3mca can also act as an organic catalyst in the polymerization of benzoxazines [19]. These are just a few examples that demonstrate the versatility of 3mca applications. Such versatility is due, among other factors, to the ability of the 3mca molecule to adapt to different environments through the rotation of its four formal single bonds. This means that 3mca may potentially adopt a wide range of molecular conformations. Interestingly, X-Ray diffraction studies show the presence of only one conformation [20] in the crystal. The same conformation is observed for 3mca bound to TraR protein present in the *Agrobacterium tumefaciens* [14]. However, a higher variety of conformations have been observed also in the structures of 3mca acting as a chelating agent in the formation of complexes with rare earth elements [17,18].

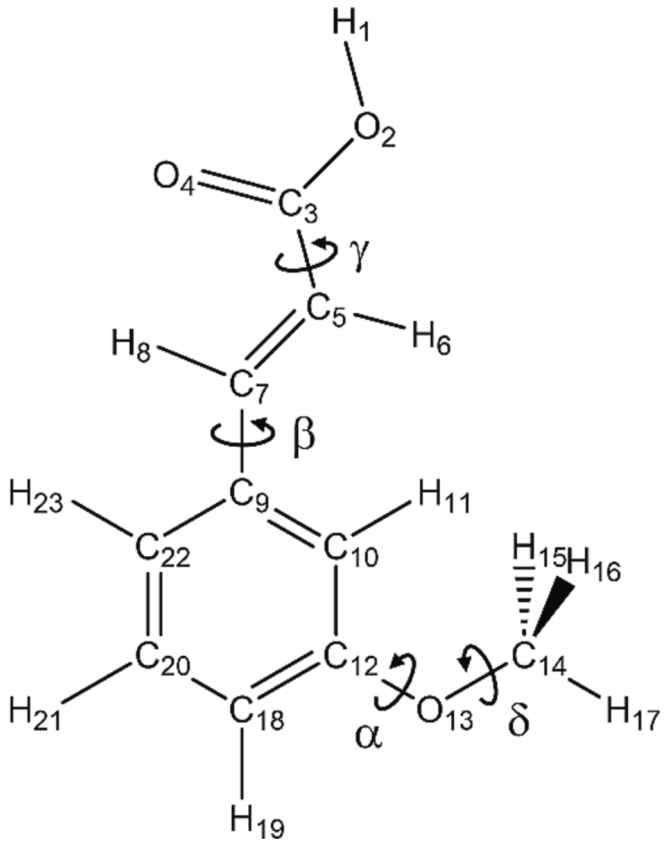

Fig. 1. The trans-3-methoxy-cinnamic acid molecule, atom labelling scheme and possible torsional coordinates. Only α, β, and γ rotations lead to different conformations.

Given the biological and chemical importance of 3mca in close relationship with the capacity of its structure to adopt different conformations, in this work we have carried out a theoretical and experimental study to determine the conformational panorama of 3mca in the gas phase. In these conditions the molecules are virtually isolated and show their intrinsic structure, from which reference conformations can be obtained. These are essential to compare with the structures of the molecule in condensed phase, subjected to different types of interactions like in molecular docking studies in proteins and nucleic acids, or to contrast predictions of theoretical calculations. The conformational study of 3mca in gas phase has been done using a combination of theoretical calculations and Fourier transform microwave spectroscopy in supersonic jets [21,22], which is described as one of the most definitive structural probes to elucidate all the conformations of a molecule [1–5]. Since 3mca is a solid with high vapor pressure, a chirped-pulse Fourier transform microwave spectrometer [23] coupled to laser ablation for the vaporization of solid samples (LA-CP-FTMW) has been used [24].

2. Methods

2.1. Experimental

A commercial sample of 3mca (m.p. 116–119 °C) was used without further purification. The milled sample was mixed with Cu powder in 1:1 w/w proportion. The homogenized mixture was pressed to form a cylindrical rod. The rotational spectrum of laser-ablated 3mca was recorded using a chirped-pulse Fourier transform microwave spectrometer (CP-FTMW) following Pate's design [23] and including a laser ablation nozzle as described elsewhere [24]. The supersonic jet was generated by expansion of Ar at a stagnation pressure of 3 bar through a 0.8 mm diameter solenoid-pulsed nozzle with molecular pulses of 900 μs duration. The sample rod was held near the exit of the nozzle in a perpendicular arrangement respect to the supersonic jet axis. Synchronized to the gas expansion a laser pulse hits the solid rod to vaporize the sample. For this purpose, the second harmonic (λ = 532 nm) of a pulsed Nd:YAG laser (Quantel Q-smart 450, 5.2 ns width, 20 mJ/pulse) was focused on the sample. A step motor rotates and translates the rod so that each laser pulse hits the rod at a fresh surface. For each combined gas/laser pulse 8 measurement cycles are performed to decrease the measurement time and sample consumption. To achieve this, an AWG waveform generates an 8 frames signal with the chirp polarization pulses. Each chirp is amplified by a 200 W peak power pulsed traveling wave tube amplifier and the corresponding FID signals are acquired in the time domain during 40 μs after each polarization pulse. Under these conditions 520 000 spectra were coadded and averaged. The resulting spectrum was assigned and measured using JB95 [25] program and the AABS package [26] available as well as many other useful applications

on the PROSPE website [27]. The measured spectra were finally analyzed using Pickett's SPCAT/SPFIT suite of programs [28].

2.2. Computational

The conformational panorama of 3mca has been first explored using the Conformer-Rotamer Ensemble Sampling Tool program (CREST) [29]. The eight different conformers found were further optimized at B3LYP-D3BJ/6–311++G(2d,p) [30–32] level including the Grimme D3 [33] empirical dispersion corrections and the Becke-Johnson BJ damping function [34]. Frequency calculations within the harmonic approximation have been carried out at B3LYP-D3BJ/6–311++G(2d,p) to confirm that the structures obtained correspond to energetic minima. The conformers shown in Fig. 2 were labelled from C1 to C8, in increasing order of electronic energy. Additionally, conformers are also labelled according to the configurations resulting from rotation following α, β, and γ coordinates (Fig. 1). For the first we consider the two possible configurations *entgegen* (*e*) or *zusammen* (*z*) of the methoxy group with respect to the propenoic acid group (α torsion). For the second the *e*-*z* arrangement of the C-COOH group relative to the methoxy group (β torsion). In the third case the position of the OH carboxyl group relative to the methoxy group (γ torsion). The calculated energies, spectroscopic constants and electric dipole moment components are given in Table 1 and the corresponding structures in Tables S1-S8. Further optimizations were carried out at B3LYP-D3BJ/aug-cc-pVTZ [35] and MP2/6–311++G(2d,p) [36] levels to test different computational levels. The results of these calculations are given in the supplementary information (Tables S9-S10).

The potential energy barriers for the rotation around the four simple bonds shown in Fig. 1 were explored for the most stable conformer at B3LYP-D3BJ/6–311++G(2d,p) level by doing relaxed scans along the appropriate coordinates as shown in Figs. S1-S4. All the calculations have been performed with the Gaussian 16 program [37]. The possible intramolecular interactions have been investigated through quantum theory of atoms in molecules (QTAIM) [38] and non-covalent interactions analysis (NCI) [39] using the Multiwfn program [40].

3. Results and discussion

3.1. Microwave spectra

The rotational spectrum of 3mca is shown in Fig. S5 where it is compared with the eight spectra predicted from the theoretically calculated structures. All the predicted conformers are asymmetric rotors close to the prolate limit ($\kappa = -1$), having reasonably high values of the μ_a electric dipole moment component. The assignment of the spectra was based on the identification of R-branch *a*-type lines which are expected to appear forming groups with characteristic patterns separated by $B + C$ (see Fig. S5). In this way, the spectra of eight conformers were unequivocally identified as shown in Fig. 3. *a*-Type lines were measured

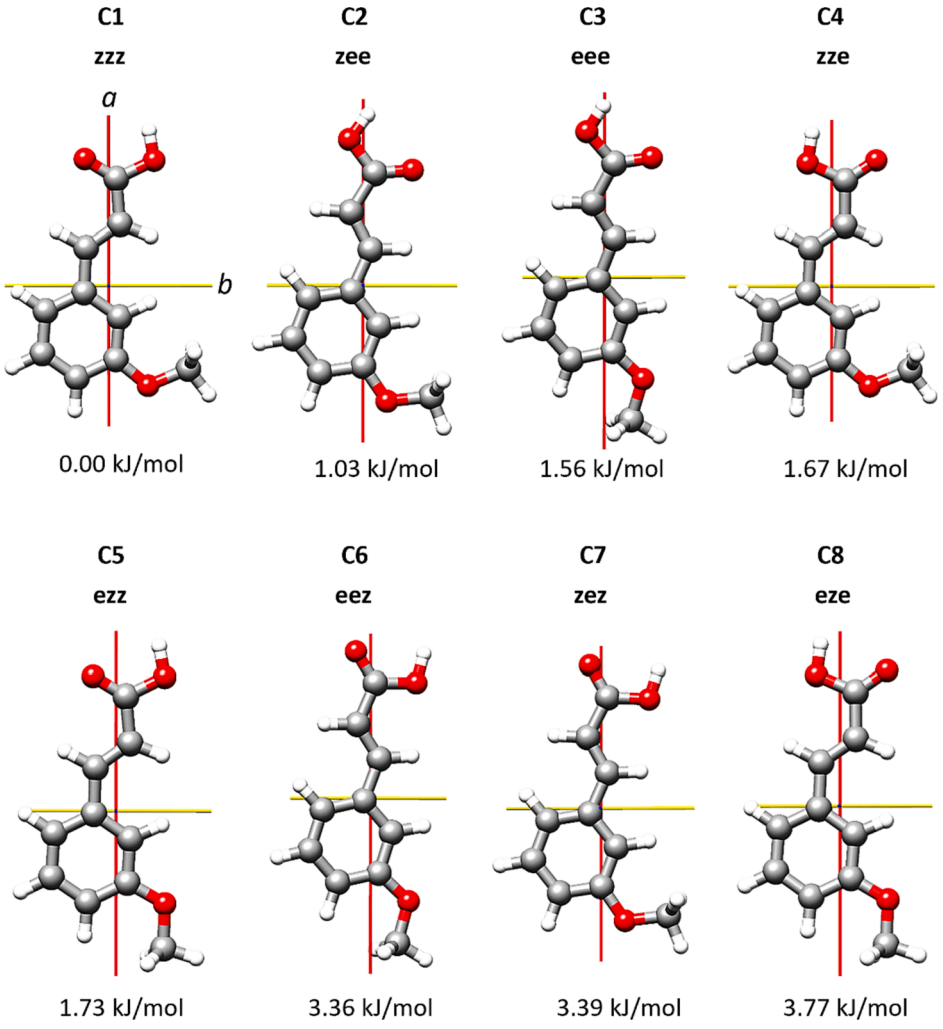

Fig. 2. Conformers predicted at B3LYP-D3BJ/6–311++G(2d,p) level. The *a* (red) and *b* (yellow) inertial axes are shown. Below each conformer the energies relative to the most stable conformer C1 are given. (For interpretation of the references to colour in this figure legend, the reader is referred to the web version of this article.)

Table 1
Theoretical values of the spectroscopic parameters of interest calculated at B3LYP-D3BJ/6–311++G(2d,p) level for the eight conformers of the 3mca.

Parameters [a]	C1 zzz	C2 zee	C3 eee	C4 zze	C5 ezz	C6 eez	C7 zez	C8 eze
ΔE / kJ/mol	0.00	1.03	1.56	1.67	1.73	3.36	3.39	3.77
ΔE_{ZPC} / kJ/mol	0.00	0.81	1.39	1.63	1.56	3.17	3.08	3.52
ΔG (298.15 K, 1 atm) / kJ/mol	0.00	0.28	1.09	1.49	1.27	2.78	2.16	3.02
A / MHz	1457.9	1772.2	2416.9	1470.0	1859.0	2377.8	1749.3	1883.5
B / MHz	376.8	337.2	302.5	377.7	330.7	305.6	341.2	331.3
C / MHz	300.0	283.8	269.3	301.1	281.2	271.3	286	282.3
μ_a / D	2.0	1.7	3.4	−2.1	4.0	4.5	−3.0	−4.0
μ_b / D	−1.8	0.4	2.1	−1.0	−0.6	−0.4	2.0	−2.3
μ_c / D	0.0	0.0	0.0	0.0	0.0	0.0	0.0	0.0
κ	−0.87	−0.93	−0.97	−0.87	−0.94	−0.97	−0.92	−0.94
P_a / uÅ^2	1339.55	1497.07	1669.27	1336.52	1526.74	1652.15	1479.58	1523.78
P_b / uÅ^2	345.03	283.56	207.49	342.19	270.24	210.93	287.29	266.71
P_c / uÅ^2	1.61	1.61	1.61	1.61	1.61	1.61	1.61	1.61

[a] ΔE, ΔE_{ZPC} and ΔG are the electronic, zero point corrected, and Gibbs energies relative to C1. A, B and C are the rotational constants. μ_a, μ_b and μ_c are the electric dipole moment components (1 D = 3.33564 • 10^{-30} Cm).κ is the Raýs asymmetry parameter, $\kappa = (2B\text{-}A\text{-}C)/(A\text{-}C)$. P_a, P_b and P_c are the planar moments of inertia ($P_c = ½(I_a + I_b\text{-}I_c)$).

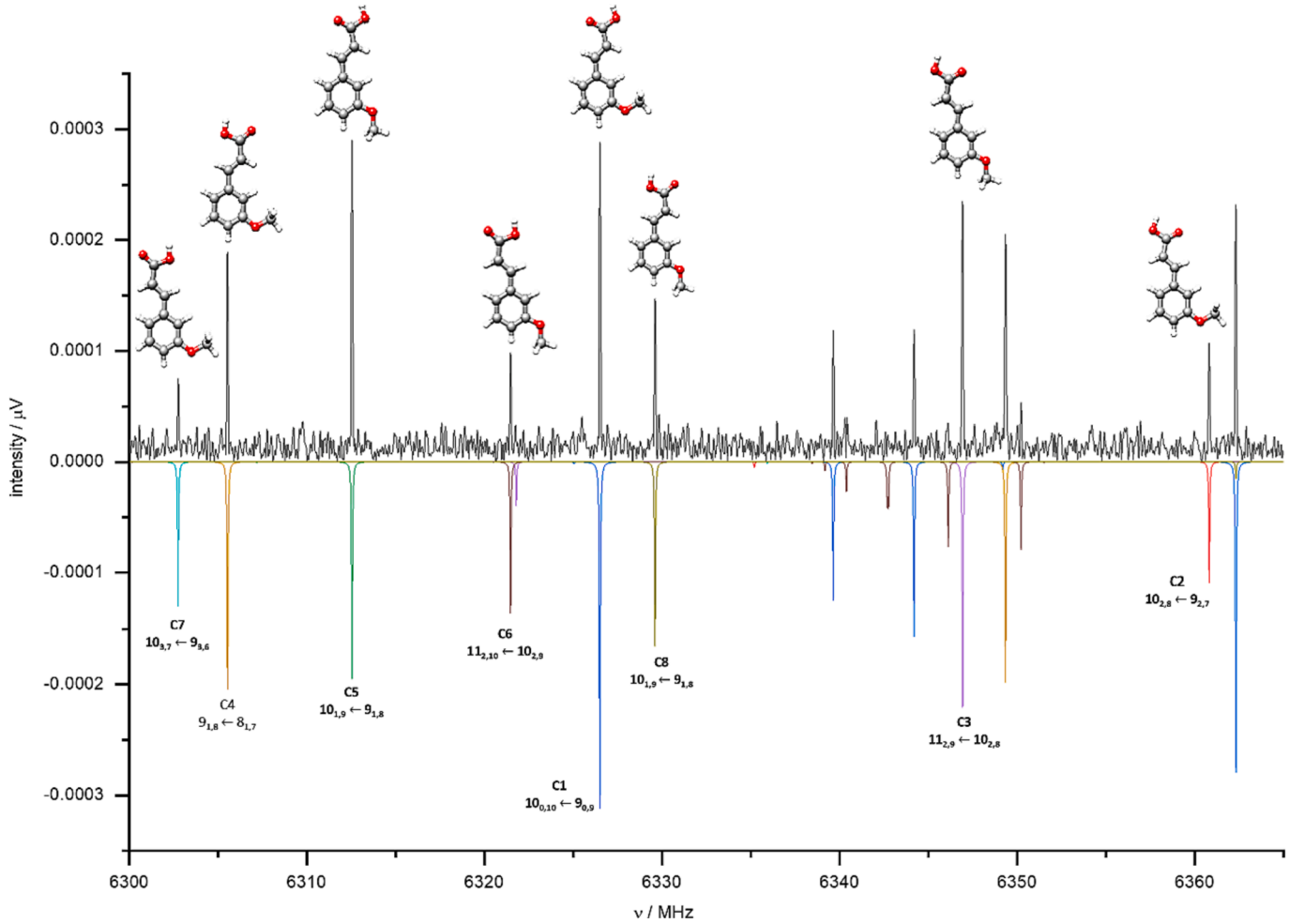

Fig. 3. A portion of the rotational spectrum of 3mca showing at least one *a*-type line assigned to each of the eight observed conformers. The upper trace is the experimental spectrum, the lower traces show the spectra predicted with the set of spectroscopic parameters of Table 2: C1 (blue), C2 (red), C3 (violet), C4 (orange), C5 (green), C6 (brown), C7 (light blue), C8 (olive). (For interpretation of the references to colour in this figure legend, the reader is referred to the web version of this article.)

in all cases, *b*-type spectra were observed for seven of them. No *c*-type spectra were observed with the predicted electric dipole moment values (see Table 1). The measured lines were fitted using the S-reduced semirigid rotor Hamiltonian of Watson in the I^r representation [41]. Only some of the quartic centrifugal distortion constants ought to be floated. The experimental spectroscopic parameters are given in Table 2. The observed frequencies are collected in Tables S12-S19.

The assignment of the observed spectra to the different conformers of

Table 2
Experimental parameters obtained for the eight 3mca conformers observed.

Parameters[a]	C1	C2	C3	C4
A / MHz	1453.97067(37)[b]	1773.279(25)	2409.04379(29)	1465.84869(72)
B / MHz	376.337403(87)	336.13666(19)	301.910412(63)	377.19836(12)
C / MHz	299.742029(81)	283.311303(89)	268.953005(58)	300.80286(13)
D_J / kHz	0.00482(40)	[0.0]	0.00170(20)	0.00367(64)
D_{JK} / kHz	[0.0][c]	0.0244(58)	−0.0096(18)	[0.0]
D_K / kHz	0.101(20)	13.1(51)	[0.0]	[0.0]
κ	−0.87	−0.93	−0.97	−0.87
P_a / uÅ^2	1340.67483(43)	1501.1628(27)	1671.60709(39)	1337.57747(66)
P_b / uÅ^2	345.37200(43)	282.6668(27)	207.45390(39)	342.52325(66)
P_c / uÅ^2	2.21347(43)	2.3301(27)	2.33021(39)	2.24569(66)
μ_a / μ_b / μ_c	+/+/-	+/+/-	+/+/-	+/+/-
N	140	63	106	69
σ / kHz	4.8	5	3.3	5.5
n_i/n_1	1	0.9(2)	0.5(1)	0.6(1)
% population	25(9)	22(7)	12(4)	16(5)
Parameters	C5	C6	C7	C8
A / MHz	1845.3041(37)	2370.992(42)	1750.5600(13)	1869.0798(34)
B / MHz	330.776130(99)	305.03152(13)	340.11713(12)	331.44458(10)
C / MHz	281.21150(10)	270.94658(15)	285.55920(13)	282.257624(57)
D_J / kHz	0.00380(31)	0.00179(36)	0.00346(49)	[0.0]
D_{JK} / kHz	−0.0555(25)	[0.0]	[0.0]	−0.0265(58)
D_K / kHz	[0.0]	[0.0]	0.38(11)	3.79(72)
κ	−0.94	−0.97	−0.93	−0.94
P_a / uÅ^2	1525.56742(82)	1654.4468(28)	1483.49452(68)	1522.43829(66)
P_b / uÅ^2	271.58206(82)	210.7883(28)	286.29297(68)	268.05046(66)
P_c / uÅ^2	2.29101(82)	2.3626(28)	2.40270(68)	2.33880(66)
μ_a / μ_b / μ_c	+/+/-	+/-/-	+/+/-	+/+/-
N	80	55	72	45
σ / kHz	3.8	4.3	5	4.5
n_i/n_1	0.31(6)	0.16(4)	0.37(8)	0.13(3)
% population	8(3)	4(1)	9(3)	3(1)

[a] A, B, and C are the rotational constants. D_J, D_{JK}, and D_K are the quartic centrifugal distortion constants in the S-reduced semirigid rotor Hamiltonian of Watson. κ is the Ray's asymmetry parameter, $\kappa = (2B\text{-}A\text{-}C)/(A\text{-}C)$. P_a, P_b and P_c are the planar moments of inertia (*i.e.,* $P_c = ½(I_a+I_b\text{-}I_c)$). $\mu_a/\mu_b/\mu_c$ indicate the electric dipole moment transition rules observed (+) or not (-). N is the number of rotational transitions fitted. σ is the rms deviations of the fit. n_i/n_1 is the population ratio of conformer Ci relative to conformer C1. [b] Standard error is given in parentheses in units of the last digit. [c] Parameters in square brackets were fixed to zero.

3mca (see Fig. 1 and Tables 1 and 2) was done unambiguously by comparing the experimental and theoretical values of the rotational constants. The error percentage in the prediction of the rotational constants is shown in Table S11. The three levels of calculation predict satisfactorily the rotational constants since the residuals are less than 1 % in all cases, and it is worth mentioning that in most cases it is less than 0.5 %. Even so, the MP2/6–311++G(2d,p) method seems to offer slightly better predictions in general. This agreement allows us to take theoretical predictions as reasonable descriptions of the conformer structures. The values of the A rotational constant and the Ray's asymmetry parameter, κ, are very sensitive to the arrangement of the functional groups of 3mca (see Fig. 2 and Table 1). The larger/smaller values of the A rotational constant correspond to the smaller/largest possible values of I_a ($I_a = \Sigma_i m_i (b_i^2 + c_i^2)$) and thus to the arrangements with the shorter/largest average distance of the atoms to the a axis. If we classify the conformers in order of decreasing values of the A rotational constant as eee(C3) > eez(C6) > eze(C8) > ezz(C5) > zee(C2) > zez(C7) > zze (C4) > zzz(C1) the influence on this constant of the arrangement of different groups can be easily seen. The group that most contributes is the methoxy group, its *entgegen* or *zusammen* dispositions giving the two conformer groups with the highest or lowest A values, respectively. The next one is the *z-e* arrangement on the propenoic acid group, and finally the less influential is the *z-e* contribution of the carboxylic group. The observed selection rules and intensities reinforce the assignments done for the couples of conformers showing similar rotational constants. This is obvious for the couple C3/C6 since for C3 *a*- and *b*-type rotational spectra have been observed while only *a*-type rotational spectrum is observed for C6 according to the theoretical predictions (see Table 1). The relative intensities observed the *a*-type and *b*-type spectra observed for other couples as C1/C4, C2/C7, or C5/C8 with similar rotational constants are in good agreement with the squared values of the predicted electric dipole moment components.

The P_c planar moment ($P_c = (I_a + I_b\text{-}I_c)/2 = \Sigma_i m_i c_i^2$) gives a measure of the mass extension out of the *ab* inertial plane. The P_c experimental values derived from the observed rotational constants, given in Table 2 for all the observed forms, lie in the range 2.2–2.4 uÅ^2. These values are consistent with a planar skeleton of 3mca lying on the *ab* inertial plane with only two of the methyl group hydrogen atoms out-of-plane. The P_c values could also reflect the existence of out-of-plane vibrational contributions, associated to the acrylic acid and methoxy groups. The contribution of these groups can be understood if the planar moment values for anisole (P_c = 1.70 uÅ^2) [42] and trans-cinnamic acid (P_c = 0.55 uÅ^2 or 0.59 uÅ^2 depending on the orientation of the carboxyl group) [43] are considered. In anisole and trans-cinnamic acid the planar aromatic ring coincides with the *ab* inertial plane, the experimental P_c values can be interpreted as the independent contributions of the methoxy and acrylic acid groups. Adding these values, we obtain P_c = 2.25 uÅ^2 or 2.29 uÅ^2, values close to the 3mca experimental planar moments given in Table 2. Together with the non-observation of *c*-type lines these P_c values confirm the essentially planar structure of the 3mca skeleton for all conformations observed.

3.2. Relative populations and conformer stabilities

The relative population abundances of the observed conformers in the supersonic jet can be estimated from relative intensity measurements [44,45]. This is possible only if it is assumed that expansion cooling brings all the molecular systems to the lowest vibrational state of each observed conformer. While it is not possible to evaluate vibrational temperatures from our experiment since no vibrational excited states have been observed, the rotational temperatures can be estimated as described in the electronic supplementary information (see Fig. S6)

[46]. The calculated rotational temperatures, plotted in Fig. 4, are close to 1 K indicating the rotational cooling provided by the supersonic jet in the experimental conditions used is rather high.

In the jet, the intensities of the α-type lines (α = *a*, *b*, or *c*) of conformer *i*, with number density n_i in the jet, can be assumed to be proportional to $(\mu_\alpha)_i^2 \cdot ni$, where $(\mu_\alpha)_i$ is the electric dipole moment component along the α principal inertial axis for conformer *i*. By combining the relative intensities measured on different *a*-type transitions common to all conformers (see Table S20) with the theoretically predicted values of μ_a (see Table 1) we have estimated the relative abundances of the observed conformers in the jet as given in Table S20. In this Table and in Fig. 5a the estimated population distribution in the jet is compared to that calculated theoretically at 298 K and 1 bar from the Gibbs energies [1] for all the levels of calculation used. The theoretical calculations show good agreement between them except for conformer C7 predicted at the MP2 level to be the most populated at room temperature in contrast with the experimental results and the DFT predictions. The reason for this discrepancy may lie in the predicted low value of the harmonic frequency for the lowest frequency vibrational mode, the torsion of the propenoic acid group around its bond to the aromatic ring associated with β coordinate ($\beta = \angle C_5\text{-}C_7\text{-}C_9\text{-}C_{10}$, Fig. 1). The frequency for this vibration is predicted to be 7.6 cm^{-1} at MP2/6–311++G(2d,p) for C7 form, while for the other conformers is predicted to be 15.2 cm^{-1} for C2 and in the range 20–24 cm^{-1} for the other forms. The DFT computations predict a frequency of 22.2 cm^{-1} (6–311++G(2d,p)) or 25.6 cm^{-1} (aug-cc-pVTZ) for C7 and values in the range 24–31 cm^{-1} for the other forms.

The observed relative abundance of conformers in the supersonic expansion results in this case from a series of successive processes starting from the laser vaporization, the seeding of molecules in the region where the laser ablation plume and the carrier gas stream cross each other, and the collisional cooling occurring in the subsequent supersonic expansion which we have proved it is successful concerning rotational temperature. Laser ablation may induce high temperatures followed by the subsequent cooling. The relative population of the different conformers of 3mca would be brought close to that of thermodynamic equilibrium at the local temperature and pressure of the carrier gas in the seeding region, just at the initial stages of the expansion, only if a high collision rate exists in the seeding region where the laser ablation plume and the expansion stream cross each other [47].

Using the B3LYP-D3BJ/6–311++G(2d,p) vibrational and rotational data, we have analyzed the temperature and pressure dependence of the equilibrium relative populations. These have a small dependence on pressure but are sensitive to temperature especially concerning the most abundant conformers, as can be seen in Fig. S7 and in Fig. 5. The populations observed in the supersonic jet seem to show better agreements with temperatures lower than ambient temperature. We do not know the amount of each form in the solid sample used. A previous X-ray diffraction study of 3mca crystalized in the γ-form shows is composed exclusively by conformer C8 units. Laser ablation may provide enough energy to bring molecules to high energy vibrational excited states allowing thermal redistribution among the different possible conformers if a high collisional rate exists in the seeding region. In this case the observation of a population ratio corresponding to equilibrium at a temperature lower than the stagnation temperature can be reasonable. In Fig. 5b the experimental estimated percent populations are compared to those calculated at 273.15 K. The small discrepancies can be reasonable if we consider the quoted errors and the theoretical approximations. However, the discrepancies are not incompatible with the existence of partial vibrational relaxation in the supersonic jet. In fact, conformers C1, C2, C4 and C7, seem to have a higher population than that predicted, while C3, C5, C6 and C8 are less populated than predicted. Relaxation in the supersonic expansion form may occur when two non-equivalent conformers and the corresponding two minima in the potential energy surface can interconvert through a small barrier around 400 cm^{-1} [48]. To test the possible paths for conformational relaxation, the potential energy barriers corresponding to the rotation around the four single bonds shown in Fig. 1 (coordinates α, β, γ and δ), which allow the interconversion between the eight observed conformers were explored at the B3LYP-D3BJ/6–311++G(2d,p). As can be seen in Figures S1-S4, energy barriers were found to be: 240 cm^{-1} (α), 446 cm^{-1} (β), 644 cm^{-1} (γ) and 1079 cm^{-1} (δ). The lowest interconversion barrier corresponds to the methoxy group torsion (α, Fig. S1). The observation of all the predicted forms indicates that there is not a total relaxation, but the data can be compatible with a partial relaxation following the methoxy group torsion path as indicated in Fig. 5b: C5 → C1, C3 → C2, C8 → C4, C6 → C7. It is also interesting to note that conformers C1, C2, and C4, the most populated conformers, reach the lower rotational temperatures (see Fig. 4).

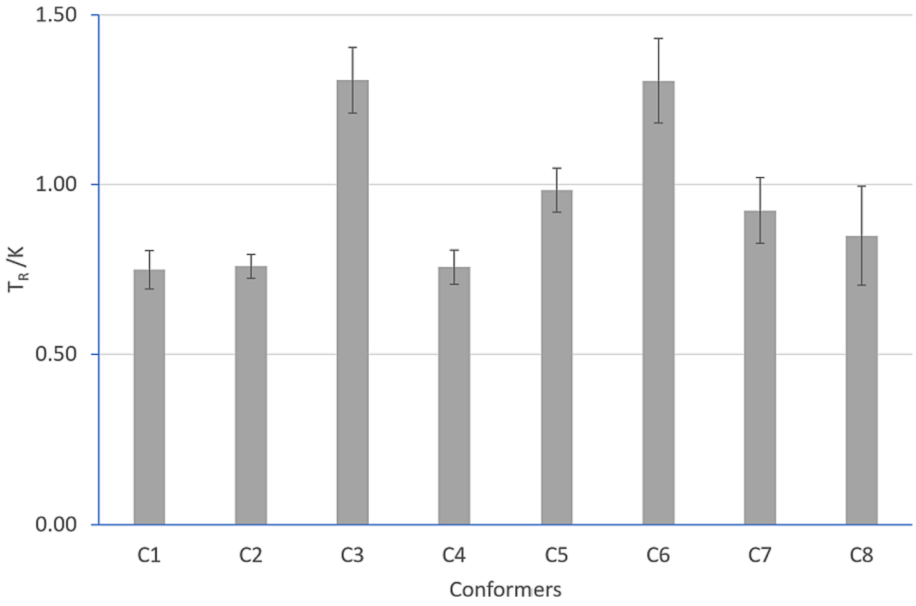

Fig. 4. Rotational temperatures (T_R) reached in the supersonic jet for the observed conformers of 3mca obtained from the measured line [46]. The error bars reflect the standard deviation of the fit to determine T.

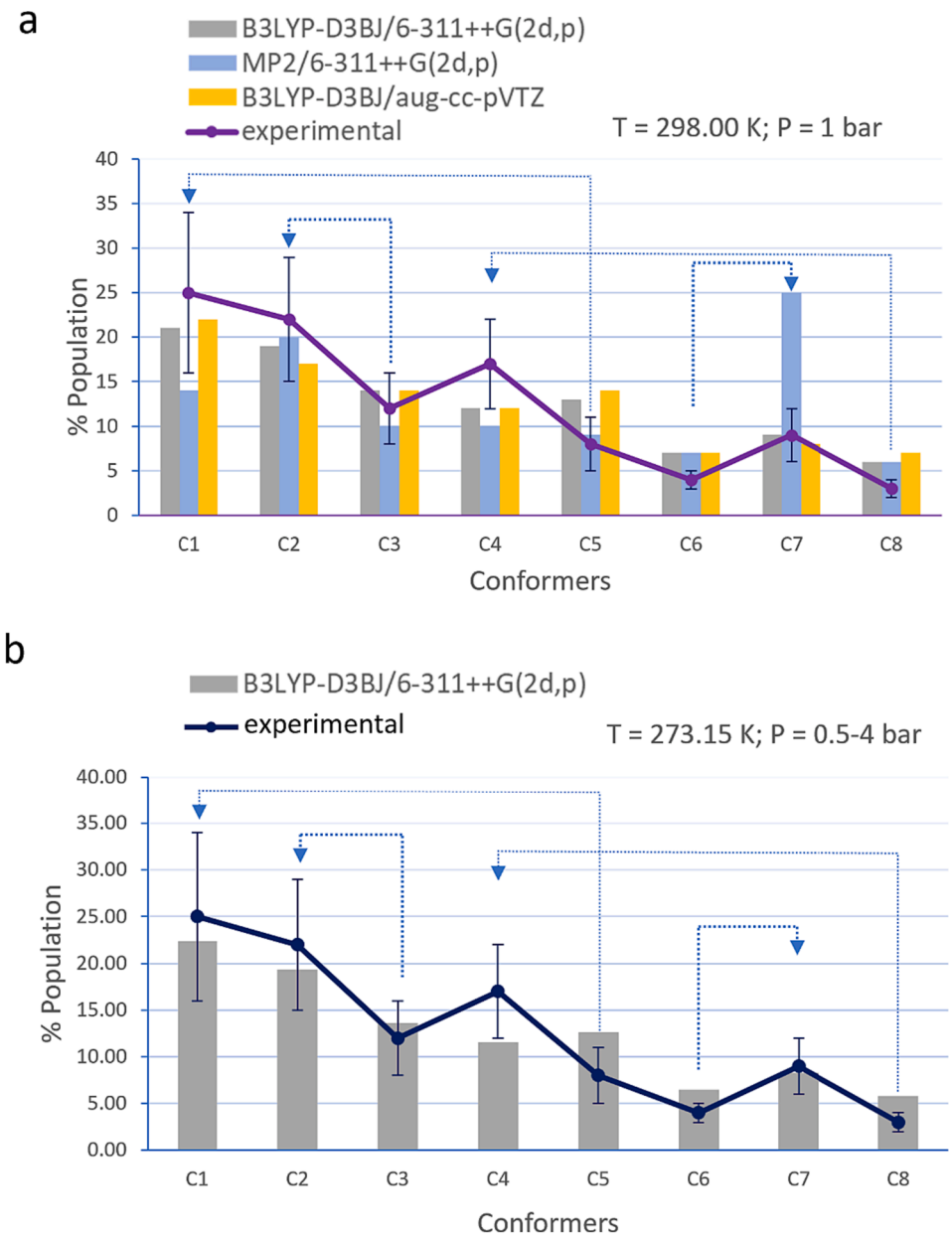

Fig. 5. Comparison of the relative percent populations of the observed 3mca conformers, estimated from relative intensity measurements of sets of common rotational *a*-type lines, with the hypothetical equilibrium gas phase populations calculated from Gibbs energies. In plot a, the percent populations at 1 bar and 298 K calculated at the three theoretical levels used are shown. In plot b, the B3LYP-D3BJ/6–311++G(2d,p) data were used to calculate the populations at 273.15 K. The calculated populations are independent of pressure in a wide range below 4 bar. In plots a and b, the plausible paths for partial collisional relaxation in the supersonic jet due to methoxy group torsion (α) (see Figures 1 and S1) are indicated as arrows.

3.3. Correlation between gas phase and condensed phase structures

Given the good agreement between the observed and calculated rotational parameters the structures predicted theoretically (Tables S1-S8) can be taken as a reasonable description of the experimental structures for isolated 3mca. The results on the relative intensity measurements also indicate that the theoretical results give a reasonable description of the stability of the different forms of 3mca. It is difficult to establish the origin of relative stability between conformers giving the small energy differences between them. All the conformers have predicted energies below 400 cm^{-1} relative to conformer C1. The QTAIM [38] analysis do not anticipate any other bond than the covalent ones and the NCI analysis [39] (see Fig. S8) predict similar small interactions of attractive and repulsive nature in all the complexes. There are no clear correlations between the predicted energies and the configurations of the functional groups, so the results may arise from the balance of the different covalent and non-covalent forces stabilizing the different forms.

It is interesting to compare the observed conformations with those reported in the literature corresponding to condensed phases. The structure of the *γ*-form crystal of 3mca [20] shows just one conformer which correlates with conformer C8 (see Fig. 2), the least stable form observed in gas phase. The same conformer is found when 3mca interacts with TraR protein [14]. Packing effects and different intermolecular interactions seem to favour C8 conformer in the crystal and also as bioactive configuration. Interestingly, in coordination compounds with lanthanides [17,18] where 3mca is in its anionic form and it is not possible to distinguish the two configurations associated with the acid group, other configurations which can be correlated with gas phase forms C1/C6, C4/C7 or C3/C8 are found. In a study on the influence of

different ligands in the growth of lanthanide phosphate nanoparticles [49], a configuration between C1 and C4 with the methoxy group being perpendicular to the ring plane has been observed. In any case, the widest conformational landscape could only be observed in gas phase using microwave spectroscopy.

4. Conclusions

In this work we have observed the spectra of a total of eight rotamers of 3mca in the isolation conditions of a supersonic jet seeded with 3mca after its laser-vaporisation. The observed rotamers have been identified from the rotational parameters with the eight possible predicted forms of 3mca. The relative abundances of the eight conformers in the supersonic jet have been estimated from relative intensity measurements and the calculated electric dipole moment components at B3LYP-D3BJ/6–311++G(2d,p) level (see Table 1). These abundances are consistent with the hypothetical equilibrium relative populations at temperatures lower than the stagnation temperature of the expanding gas.

The comparison of isolation structures with condensed phase structures reaffirms that the relative stability of the conformers of a molecule in absence of interactions cannot be extrapolated to condensed phase. However, it can be easily shown that the conformers found in condensed phase correlate and are accessible to the molecule from those found in gas phase. For example, conformer C8 is accessible to the molecule from any of the gas phase forms by simple rotation about single bonds with small energy cost. The contrary is also true, since in this work we have started with a solid sample with 3mca presumably in the C8 form to obtain in the supersonic expansion a conformer distribution close to that calculated for equilibrium in the gas phase at temperatures lower than the stagnation temperature of the expanding gas. This means that the amount of energy provided by laser ablation together with the collisions with the expanding gas can bring the different forms to get a population distribution close to that at equilibrium at some point upstream the supersonic expansion. From this point, cooling in the jet brings the molecules to the lowest vibrational state of each conformer. Although we cannot determine the vibrational temperatures, rotational states population cools down to *ca.* 1 K.

CRediT authorship contribution statement

Roger Castillo: Data curation, Investigation, Writing – original draft, Writing – review & editing. **Susana Blanco:** Conceptualization, Data curation, Formal analysis, Funding acquisition, Methodology, Project administration, Validation, Writing – original draft, Writing – review & editing, Investigation, Supervision. **Juan Carlos López:** Conceptualization, Data curation, Formal analysis, Funding acquisition, Methodology, Project administration, Validation, Writing – original draft, Writing – review & editing, Investigation, Supervision.

Declaration of competing interest

The authors declare that they have no known competing financial interests or personal relationships that could have appeared to influence the work reported in this paper.

Data availability

Data will be made available on request.

Acknowledgements

The authors acknowledge the Ministerio de Ciencia e Innovación (Grant PID2021-125207NB-C33) and the Junta de Castilla y León (Grant INFRARED-FEDER IR2020-1-UVa02). R.C. acknowledges the Fundación Banco de Santander for financial support (Grant Programa Iberoamérica/Universidad de Valladolid 2022-23).

Appendix A. Supplementary data

Supplementary data to this article can be found online at https://doi.org/10.1016/j.saa.2024.123997.

References

[1] S. Blanco, J.C. López, S. Mata, J.L. Alonso, Conformations of γ-Aminobutyric Acid (GABA): The Role of the n→π* Interaction, Angew. Chem. Int. Ed. 49 (2010) 9187–9192, https://doi.org/10.1002/ANIE.201002535.
[2] J.C. López, C. Pérez, S. Blanco, V.A. Shubert, B. Temelso, G.C. Shields, M. Schnell, Water induces the same crown shapes as Li+ or Na+ in 15-crown-5 ether: A broadband rotational study, Phys. Chem. Chem. Phys. 21 (2019) 2875–2881, https://doi.org/10.1039/c8cp05552a.
[3] F. Gámez, B. Martínez-Haya, S. Blanco, J.C. López, J.L. Alonso, Microwave spectroscopy and quantum chemical investigation of nine low energy conformers of the 15-crown-5 ether, Phys. Chem. Chem. Phys. 14 (2012) 12912–12918, https://doi.org/10.1039/c2cp41635b.
[4] S. Blanco, M.E. Sanz, J.C. López, J.L. Alonso, Revealing the multiple structures of serine, Proc. Natl. Acad. Sci. U S A. 104 (2007) 20183–20188, https://doi.org/10.1073/pnas.0705676104.
[5] J.L. Alonso, J.C. López, Microwave spectroscopy of biomolecular building blocks, Top. Curr. Chem. 364 (2015) 335–401, https://doi.org/10.1007/128_2014_601.
[6] C.R. Groom, I.J. Bruno, M.P. Lightfoot, S.C. Ward, IUCr, The Cambridge Structural Database, Acta Crystallographica Section B 72 (2016) 171–179, https://doi.org/10.1107/S2052520616003954.
[7] H.M. Berman, J. Westbrook, Z. Feng, G. Gilliland, T.N. Bhat, H. Weissig, I. N. Shindyalov, P.E. Bourne, The Protein Data Bank, Nucleic Acids Res. 28 (2000) 235–242, https://doi.org/10.1093/nar/28.1.235.
[8] A.J. Cruz-Cabeza, J. Bernstein, Conformational polymorphism, Chem Rev. 114 (2014) 2170–2191, https://doi.org/10.1021/cr400249d.
[9] K.A. Brameld, B. Kuhn, D.C. Reuter, M. Stahl, Small molecule conformational preferences derived from crystal structure data. A medicinal chemistry focused analysis, J. Chem. Inf. Model. 48 (2008) 1–24, https://doi.org/10.1021/CI7002494.
[10] M. Gür, H. Muğlu, M.S. Çavuş, A. Güder, H.S. Sayıner, F. Kandemirli, Synthesis, characterization, quantum chemical calculations and evaluation of antioxidant properties of 1,3,4-thiadiazole derivatives including 2- and 3-methoxy cinnamic acids, J. Mol. Struct. 1134 (2017) 40–50, https://doi.org/10.1016/J.MOLSTRUC.2016.12.041.
[11] T.T. Thuy, B.T. Cham, N. Thi, T. Linh, P. Thi, N. Bich, S. Adorisio, D.V. Delfino, Phenolic Acid Analogues from Balanophora laxiflora Inhibit Proliferation of In Vitro Acute Myeloid Leukemia Cells, Nat. Prod. 16 (2022) 253–258, https://doi.org/10.25135/rnp.273.2106.2117.
[12] Y.X. Ge, Y.H. Wang, J. Zhang, Z.P. Yu, X. Mu, J.L. Song, Y.Y. Wang, F. Yang, N. Meng, C.S. Jiang, H. Zhang, New cinnamic acid-pregenolone hybrids as potential antiproliferative agents: Design, synthesis and biological evaluation, Steroids. 152 (2019) 108499, https://doi.org/10.1016/J.STEROIDS.2019.108499.
[13] M. Okulus, M. Rychlicka, A. Gliszczyńska, Enzymatic production of biologically active 3-methoxycinnamoylated lysophosphatidylcholine via regioselctive lipase-catalyzed acidolysis, Foods 11 (2022) 7, https://doi.org/10.3390/FOODS11010007.
[14] D. Pan, X.Y. Wang, J.W. Zhou, L. Yang, A. Khan, D.Q. Wei, J.J. Li, A.Q. Jia, Virulence and biofilm inhibition of 3-methoxycinnamic acid against Agrobacterium tumefaciens, J. Appl. Microbiol. 133 (2022) 3161–3175, https://doi.org/10.1111/JAM.15774.
[15] N. Ruwizhi, B.A. Aderibigbe, Cinnamic Acid Derivatives and Their Biological Efficacy, Int. J. Mol. Sci. 21 (2020) 5712, https://doi.org/10.3390/IJMS21165712.
[16] A. Garcia-Jimenez, F. García-Molina, J.A. Teruel-Puche, A. Saura-Sanmartín, P. A. García-Ruiz, A. Ortiz-López, J.N. Rodríguez-López, F. Garcia-Canovas, J. Muñoz-Muñoz, Catalysis and inhibition of tyrosinase in the presence of cinnamic acid and some of its derivatives, Int. J. Biol. Macromol. 119 (2018) 548–554, https://doi.org/10.1016/J.IJBIOMAC.2018.07.173.
[17] O. Khalfaoui, A. Beghidja, C. Beghidja, Y. Guari, J. Larionova, J. Long, Synthesis, crystal structures, luminescent and magnetic properties of rare earth dinuclear complexes and one-dimensional coordination polymers supported by two derivatives of cinnamic acid, Polyhedron. 207 (2021) 115366, https://doi.org/10.1016/J.POLY.2021.115366.
[18] O. Khalfaoui, A. Beghidja, J. Long, A. Boussadia, C. Beghidja, Y. Guari, J. Larionova, Cinnamic acid derivative rare-earth dinuclear complexes and one-dimensional architectures: synthesis, characterization and magnetic properties, J. Chem. Soc. Dalton Trans. 46 (2017) 3943–3952, https://doi.org/10.1039/C7DT00326A.
[19] R.B. Rodríguez, D. Iguchi, R. Erra-Balsells, M. Laura Salum, P. Froimowicz, Design and Effects of the Cinnamic Acids Chemical Structures as Organocatalyst on the Polymerization of Benzoxazines, Polymers 12 (2020) 1527, https://doi.org/10.3390/POLYM12071527.
[20] S.D.M. Atkinson, M.J. Almond, G.A. Bowmaker, M.G.B. Drew, E.J. Feltham, P. Hollins, S.L. Jenkins, K.S. Wiltshire, The photodimerisation of the chloro-, methoxy- and nitro-derivatives of trans-cinnamic acid: a study of single crystals by vibrational microspectroscopy, J. Chem. Soc., Perkin Trans. 2 (2002) 1533–1537, https://doi.org/10.1039/B205116H.
[21] B.H. Pate, Taking the Pulse of Molecular Rotational Spectroscopy, Science 333 (2011) 947–948, https://doi.org/10.1126/science.1207994.

[22] W. Caminati, J.-U. Grabow, Microwave Spectroscopy: Molecular Systems, Frontiers of Molecular Spectroscopy (2009) 455–552, https://doi.org/10.1016/B978-0-444-53175-9.00015-5.
[23] G.G. Brown, B.C. Dian, K.O. Douglass, S.M. Geyer, S.T. Shipman, B.H. Pate, A broadband Fourier transform microwave spectrometer based on chirped pulse excitation, Rev. Sci. Instrum. 79 (2008) 4–5, https://doi.org/10.1063/1.2919120.
[24] S. Blanco, A. Macario, J.C. López, The structure of isolated thalidomide as reference for its chirality-dependent biological activity: a laser-ablation rotational study, Phys. Chem. Chem. Phys. 23 (2021) 13705–13713, https://doi.org/10.1039/D1CP01691A.
[25] D.F. Plusquellic, Jb95 Spectral fitting program, NIST, Gaithersburg, https://www.nist.gov/services-resources/software/jb95-spectral-fitting-program.
[26] Z. Kisiel, Assignment and analysis of complex rotational spectra, in: Spectroscopy from Space, Springer, Netherlands, Dordrecht, 2001, pp. 91–106, https://doi.org/10.1007/978-94-010-0832-7_6.
[27] Z. Kisiel, PROSPE. Programs for Rotational Spectroscopy. http://info.ifpan.edu.pl/~kisiel/prospe.htm.
[28] H.M. Pickett, The fitting and prediction of vibration-rotation spectra with spin interactions, J. Mol. Spectrosc. 148 (1991) 371–377, https://doi.org/10.1016/0022-2852(91)90393-O.
[29] P. Pracht, F. Bohle, S. Grimme, Automated exploration of the low-energy chemical space with fast quantum chemical methods, Phys. Chem. Chem. Phys. 22 (2020) 7169–7192, https://doi.org/10.1039/c9cp06869d.
[30] C. Lee, W. Yang, R.G. Parr, Development of the Colle-Salvetti correlation-energy formula into a functional of the electron density, Phys. Rev. B 37 (1988) 785–789, https://doi.org/10.1103/PHYSREVB.37.785.
[31] A.D. Becke, Density-functional thermochemistry, III. The role of exact exchange, J. Chem. Phys. 98 (1993) 5648, https://doi.org/10.1063/1.464913.
[32] M.J. Frisch, J.A. Pople, J.S. Binkley, Self-consistent molecular orbital methods 25. Supplementary functions for Gaussian basis sets, J. Chem. Phys. 80 (1984) 3265–3269, https://doi.org/10.1063/1.447079.
[33] S. Grimme, J. Antony, S. Ehrlich, H. Krieg, A consistent and accurate ab initio parametrization of density functional dispersion correction (DFT-D) for the 94 elements H-Pu, J. Chem. Phys. 132 (2010) 154104, https://doi.org/10.1063/1.3382344.
[34] S. Grimme, S. Ehrlich, L. Goerigk, Effect of the damping function in dispersion corrected density functional theory, J. Comput. Chem. 32 (2011) 1456–1465, https://doi.org/10.1002/jcc.21759.
[35] T.H. Dunning, Gaussian basis sets for use in correlated molecular calculations. I. The atoms boron through neon and hydrogen, J. Chem. Phys. 90 (1998) 1007, https://doi.org/10.1063/1.456153.
[36] C. Møller, M.S. Plesset, Note on an approximation treatment for many-electron systems, Phys. Rev. 46 (1934) 618–622, https://doi.org/10.1103/PhysRev.46.618.
[37] M.J. Frisch et al, Gaussian 16, Revision A.03, Gaussian Inc., Wallingford CT, 2016. (2016).
[38] R.F.W. Bader, A quantum theory of molecular structure and its applications, Chem. Rev. 91 (1991) 893–928, https://doi.org/10.1021/cr00005a013.
[39] E.R. Johnson, S. Keinan, P. Mori-Sánchez, J. Contreras-García, A.J. Cohen, W. Yang, Revealing noncovalent interactions, J. Am. Chem. Soc. 132 (2010) 6498–6506, https://doi.org/10.1021/ja100936w.
[40] T. Lu, F. Chen, Multiwfn: A multifunctional wavefunction analyzer, J. Comput. Chem. 33 (2012) 580–592, https://doi.org/10.1002/jcc.22885.
[41] J.K.G. Watson, Aspects of Quartic and Sextic Centrifugal Effects on Rotational Energy Levels, in: J.R. Durig (Ed.), Vibrational Spectra and Structure a Series of Advances, Vol 6, Elsevier, New York, 1977, pp. 1–89.
[42] O. Desyatnyk, L. Pszczółkowski, S. Thorwirth, T.M. Krygowski, Z. Kisiel, The rotational spectra, electric dipole moments and molecular structures of anisole and benzaldehyde, Phys. Chem. Chem. Phys. 7 (2005) 1708–1715, https://doi.org/10.1039/B501041A.
[43] V. Cortijo, E.R. Alonso, S. Mata, J.L. Alonso, Conformational Map of Phenolic Acids, J. Phys. Chem. A 122 (2018) 646–651, https://doi.org/10.1021/acs.jpca.7b08882.
[44] G.T. Fraser, R.D. Suenram, C.L. Lugez, Rotational spectra of seven conformational isomers of 1-hexene, J. Phys. Chem. A 104 (2000) 1141–1146, https://doi.org/10.1021/JP993248N.
[45] A.S. Esbitt, E.B. Wilson, Relative Intensity Measurements in Microwave Spectroscopy, Rev. Sci. Instrum. 34 (1963) 901–907, https://doi.org/10.1063/1.1718618.
[46] J.M. Oldham, C. Abeysekera, B. Joalland, L.N. Zack, K. Prozument, I.R. Sims, G. B. Park, R.W. Field, A.G. Suits, A chirped-pulse Fourier-transform microwave/pulsed uniform flow spectrometer. I. The low-temperature flow system, J. Chem. Phys. 141 (2014) 154202, https://doi.org/10.1063/1.4903253.
[47] S. Blanco, A. Lesarri, J.C. López, J.L. Alonso, The gas-phase structure of alanine, J. Am. Chem. Soc. 126 (2004) 11675–11683, https://doi.org/10.1021/ja048317c.
[48] R.S. Ruoff, T.D. Klots, T. Emilsson, H.S. Gutowsky, Relaxation of conformers and isomers in seeded supersonic jets of inert gases, J. Chem. Phys. 93 (1990) 3142–3150, https://doi.org/10.1063/1.458848.
[49] R. Komban, K. Koempe, M. Haase, Influence of different ligand isomers on the growth of lanthanide phosphate nanoparticles, Cryst. Growth. Des. 11 (2011) 1033–1039, https://doi.org/10.1021/CG1010314/.